RSC Advances

PAPER

View Article Online
View Journal | View Issue

Cite this: *RSC Adv.*, 2020, **10**, 18192

Investigation on dispersion properties of CO_2 and ester solvent mixtures using *in situ* FTIR spectroscopy†

Zihao Yang,‡*[a] Taiheng Yin,‡[a] Fengfan Zhang,[a] Wei Wu,[a] Meiqin Lin,*[a] Zhaoxia Dong[ab] and Juan Zhang[a]

Received 12th January 2020
Accepted 29th April 2020

DOI: 10.1039/d0ra00326c

rsc.li/rsc-advances

To study the microscopic dispersion state of CO_2 in different ester solvents, the solubility, volume expansion coefficients and *in situ* Fourier transform infrared (FTIR) spectra of the CO_2–ester system were measured. The results show that the solubility and expansion coefficient of CO_2 in ester solvents decreases as the hydrocarbon chain increases. As the pressure increases, the infrared absorption peaks of CO_2 and the functional groups characteristic of ester molecules shift, indicating that CO_2 molecules interact with ester molecules and that CO_2 would destroy the interactions between the ester molecules. The hydrocarbon chain length of the ester molecules has a significant effect on the infrared absorption peak of the CO_2–ester system. As the hydrocarbon chain length increases, the CO_2 absorption peak shift and peak shift of the carbonyl groups in the ester gradually decrease.

1. Introduction

It is easy to prepare supercritical CO_2. Supercritical CO_2 is very dense, highly soluble, chemically inert, safe and nontoxic and can be separated at room temperature; thus, it has been widely used in supercritical fluid extraction.[1–7] Meanwhile, CO_2 has been used to improve oil recovery and has played an important role in petroleum production, especially in low permeability oilfields.[8–11] The dissolution of CO_2 in crude oil and the resulting volume expansion are considered to be the two major mechanisms responsible for improving oil recovery.[12–16] It is well known that both supercritical fluid extraction and CO_2 flooding are essentially equilibrium processes that occur between CO_2 and organic liquid systems under high temperatures and high pressures. Therefore, many researchers have studied the CO_2–organic liquid phase and accumulated various experimental data on the phases of CO_2 and the organic liquid systems.[17–24]

Our recent research findings have shown that, when CO_2 molecules enter an organic liquid, instead of not dissolving in the organic liquid, the CO_2 molecules are dispersed in the organic liquid in the form of molecular aggregates.[25,26] CO_2 molecules are dispersed in the organic liquid and have unique microscale morphologies. Thus, a molecular dynamics technique was used to study the radial distribution function of each molecule in mixed systems containing CO_2 and an organic liquid, which included *n*-hexane, cyclohexane, toluene and ethanol, and simulations were performed for increasing pressures, revealing the microscopic morphology of dispersed CO_2 in these four organic liquids. It is believed that, in organic liquids, the dispersion state of the CO_2 molecules (including CO_2 molecule aggregates and aggregates of CO_2 and organic liquid molecules) directly affects the volume expansion of the CO_2–organic liquid system. However, molecular dynamics can only simulate parameters such as the radial distribution function, the distortion distribution function and the interaction energy of the molecules in the system to infer the intermolecular interactions, and thus, direct experimental results cannot be obtained.

As the pressure increases in the simulation, the infrared absorption spectra of the functional groups and hydrocarbon chains of the organic molecules will change due to the influence of the CO_2 molecules. Similarly, due to the effect of the organic liquid molecules, the infrared absorption spectra of CO_2 will also change. Therefore, we can study the microscopic interactions of the molecules in the system with high-temperature and high-pressure *in situ* infrared technology. However, this technique has mainly been used to study the interactions between CO_2 and polymer molecules and between CO_2 and organic powders.[27–29] The existing experimental method cannot meet the requirements for studying the interaction between CO_2 and organic liquid molecules.[27–29] Therefore, we have improved the *in situ* infrared device and previously used the improved device

[a]*Unconventional Petroleum Research Institute, China University of Petroleum (Beijing), Beijing, 102249, People's Republic of China. E-mail: zihaoyang@cup.edu.cn; linmq@cup.edu.cn*

[b]*China University of Geosciences (Beijing), Beijing, 100083, People's Republic of China*

† Electronic supplementary information (ESI) available. See DOI: 10.1039/d0ra00326c

‡ These authors contributed equally to this work.

to measure the infrared absorption peaks of CO_2 and 2-hexanone, hexanal, and 1-hexanol under high pressures.[30]

The carbon dioxide + ester systems at high pressure are important in the separation process in a wide variety of field such as food, pharmaceutical and related industries.[31,32] Although the volumetric properties and vapor–liquid equilibrium data for carbon dioxide + ester systems at high pressure have been extensively investigated, its microscopic dispersion states are still mostly uncovered.[33–37] To further study the CO_2–organic liquid dispersion state, this study measured the solubility and volume expansion coefficient of CO_2 dispersed in esters with different hydrocarbon chains lengths under different pressures at 308.15 K and examined the effect of the hydrocarbon chain length on the solubility and volume expansion coefficient of CO_2. In addition, the *in situ* infrared absorption spectra of CO_2–ester systems under different pressure conditions were obtained to study the effects of the hydrocarbon chain length on the infrared absorption spectra of the CO_2–ester systems.

2. Experimental section

2.1. Materials

Carbon dioxide with a purity of 99.8% was purchased from Beijing Jinggao Gases Co., Ltd. Ethyl acetate (99.0%), propyl propionate (98.0%) and butyl butyrate (99.5%) were supplied by Shanghai Aladdin Bio-Chem Technology Co., Ltd.

2.2. Experimental instruments and methods

The visible pressure–volume–temperature (PVT) apparatus and *in situ* FTIR apparatus were used for the experiments. The experimental setup is shown in Fig. 1. The main body of the device included an autoclave, a supercharging system and a sampling system. The internal temperature and pressure of the autoclave were monitored by temperature sensors and pressure sensors with accuracies of ±0.1 °C and ±0.1 MPa, respectively. The volumetric accuracy of the autoclave was ±0.01 mL. The high-pressure *in situ* infrared liquid sample cell was heated by an internal thermocouple and controlled by an external controller. The maximum operating temperature was 200 °C, and the temperature accuracy was ±0.1 °C. The highest operational pressure was 10 MPa, and the pressure accuracy was 0.1 MPa. Infrared absorption data were collected from 900 cm^{-1} to 4000 cm^{-1}. The detailed device information and operating procedures can be found in our previously published papers.[18,30] Briefly, a known volume ($V_0 = 30$ mL) of ester solvent was first injected into the vacuumed PVT cell, and CO_2 was pressurized into the cell. After the system reached equilibrium, the liquid phase volume (V_1) was calculated from the image captured by the camera. Then, the mixed liquid was injected slowly into the optical cell, and the infrared spectrum of the samples was obtained by using a Bruker VERTEX 80v infrared spectrometer. Finally, the mixed liquid was taken from the cell and charged into a small steel vessel that has already been vacuumed and weighed (M_0), and the pressure of the cell is kept constant by moving the piston when discharging the organic solvent out of the cell. The mass of CO_2 dissolved in the ester solvent was calculated using the weight difference method: the mass of the steel vessel containing organic solvents and CO_2 (M_1) minus the mass of the vessel after releasing CO_2 to atmosphere (M_2). The solubility (mole fraction) of CO_2 was also calculated using these data. The volume expansion coefficient (N) of ester solvent was calculated by $N = V_1/V_0$. The measurements are repeated three times, and the results are presented as the average of the replicates.

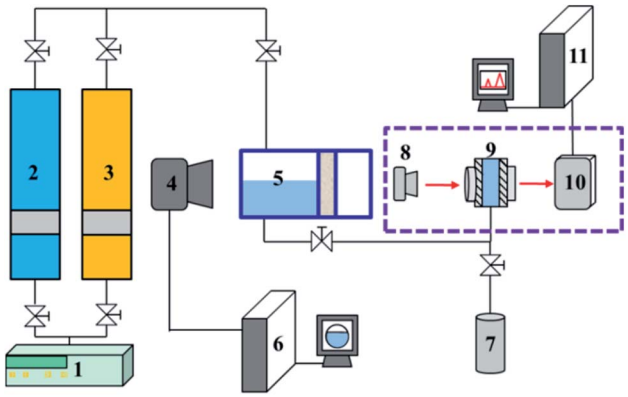

Fig. 1 Schematic of the PVT and *in situ* FTIR apparatus ((1) constant flow pump; (2) CO_2 gas bottle; (3) piston cylinder; (4) camera; (5) visible PVT cell; (6) computer; (7) little steel vessel; (8) infrared source; (9) sample optical cell; (10) infrared receptor; (11) computer).

3. Results and discussion

3.1. The solubility and volume expansion coefficient of CO_2 in the ester liquids

Fig. 2 shows the solubility and volume expansion coefficient of CO_2 in ethyl acetate, propyl propionate and butyl butyrate under different pressure conditions at 308.15 K. The CO_2 solubility and volume expansion coefficients of CO_2 and ethyl acetate, propyl propionate, and butyl butyrate increase with increasing pressure. To our knowledge, literature vapor–liquid equilibrium data for the binary mixture of CO_2 and ethyl acetate, propyl propionate, and butyl butyrate at 308.15 K are not available. The predictive Soave–Redlich–Kwong (PSRK) equation of state (EOS) was used to evaluate the vapor–liquid equilibrium behavior of CO_2 and ethyl acetate mixtures at 308.15 K.[38] There is a good agreement between the experimental data obtained here and the theoretical data obtained using the PRSK equation of state. Under the same experimental conditions, the solubility of CO_2 and the volume expansion coefficient of the CO_2–ester liquid system with different hydrocarbon chain lengths both decrease in the following order: ethyl acetate > propyl propionate > butyl butyrate. This result indicates that the hydrocarbon chain length has a relatively large impact on the solubility of CO_2 in the ester liquids and the volume expansion coefficient of the CO_2–ester liquid system.

Previous studies have shown that the solubility of CO_2 in ester liquids is closely related to the intermolecular forces between CO_2 molecules, the intermolecular forces between CO_2 and ester molecules and the intermolecular forces between ester molecules.[17,18] Ester liquids with longer chain lengths have larger contact areas for intermolecular interactions and

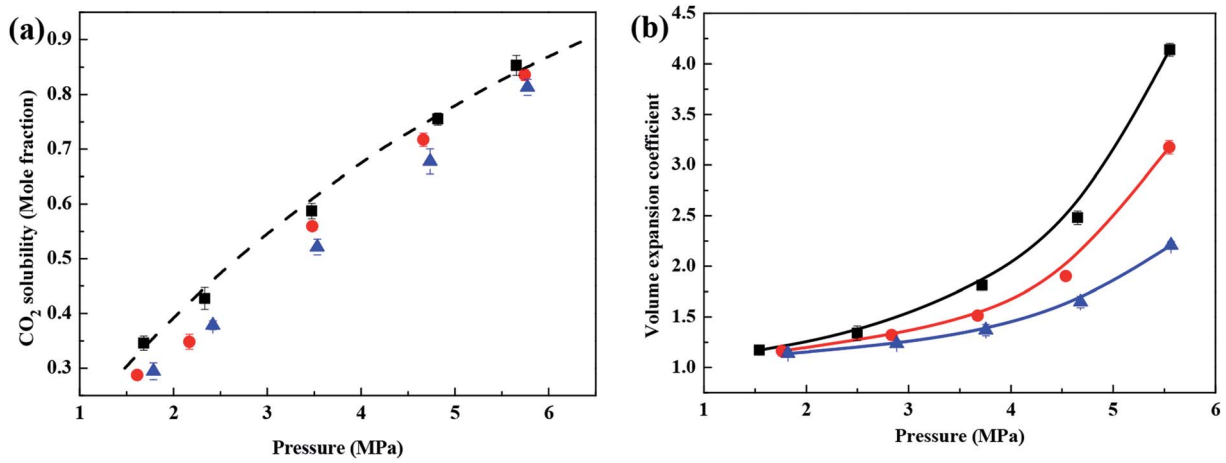

Fig. 2 (a) CO_2 solubility and (b) volume expansion coefficient of CO_2–ester liquids systems under different pressure conditions. (■) ethyl acetate, (●) propyl propionate, (▲) butyl butyrate, (– – –) PSRK EOS prediction of ethyl acetate.

stronger intermolecular forces. Under the same pressure and temperature, these stronger intermolecular forces prevent CO_2 from entering the ester liquid, leading to CO_2 being less soluble in ester liquids with longer hydrocarbon chains. On the other hand, the evaporation enthalpy of a solvent can also indirectly reflect the stability of intermolecular interactions.[30,39] The evaporation enthalpy of ethyl acetate, propyl propionate and butyl butyrate are 35.62, 42.14 and 51.12 kJ mol^{-1} respectively at 298 K.[40–43] Under the same conditions, the evaporation enthalpy decreases in the order butyl butyrate > propyl propionate > ethyl acetate, indicating that the molecular interactions of butyl butyrate are the most stable, followed by propyl propionate and ethyl acetate. This result also shows that, under the same conditions, CO_2 can more easily enter the liquid phase of ethyl acetate, thus making CO_2 more soluble in ethyl acetate than in the other two systems.

Esters with different hydrocarbon chain lengths have different distances between the ester molecules. Under the combined action of intermolecular forces, this difference in distance also causes different microscopic dispersions of CO_2 in the ester liquid, which will have a relatively large impact on the volume of the liquid system. Combined with the results of Fig. 2b, this shows that, when the temperature is constant, under the same pressure, the volume expansion is closely related to the magnitude of the intermolecular forces between the molecules of the organic liquid. The stronger the intermolecular force is, the lower the solubility of CO_2 and the smaller the expansion coefficient.[25,26] The abovementioned results indicate that the molecular structure, intermolecular forces and microscopic dispersion state of the organic liquids are the key factors affecting the solubility of CO_2 and the corresponding volume expansion coefficient of the system.

3.2. *In situ* FTIR absorption spectra of the CO_2–ester liquids systems

The *in situ* FTIR technique can be used to detect the sample changes as a function of the environment, time, temperature, and pressure. These influencing factors can cause certain regular patterns of the change in the intermolecular force and force constant of the molecules. These patterns can be reflected by *in situ* FTIR absorption peak shifts. When the intermolecular interaction is weakens, the force constant of the chemical bond will increase, and the corresponding absorption peak shifts to a higher wavenumber.[44,45] In addition, when the concentration of the detected sample is relatively low, the intensity of the absorption peak is weak; when the concentration of the sample is relatively high, the intensity of the absorption peak is high.

Fig. 3a shows the FTIR spectra of raw CO_2 and the CO_2–ethyl acetate system, which were obtained at 308.15 K and at atmospheric pressure and 7.39 MPa. Specifically, the absorption peak at 1745 cm^{-1} is characteristic of the ethyl acetate carbonyl ($\nu_{C=O}$) groups; the absorption peaks at 3704 cm^{-1}, 3600 cm^{-1} and 2314 cm^{-1} are characteristic of CO_2;[30] the absorption peak at 2989 cm^{-1} corresponds to the stretching vibration of $-CH_3$; the absorption peaks at 1490 cm^{-1} and 1350 cm^{-1} are attributed to the bending vibrations of $-CH_2$ and $-CH_3$. At 7.39 MPa, intense CO_2 absorption peaks are observed at 3704 cm^{-1}, 3600 cm^{-1} and 2314 cm^{-1} in the CO_2–ethyl acetate system and no such peaks are detected at atmospheric pressure. This finding indicates that, when the pressure increases from atmospheric pressure to 7.39 MPa, the CO_2 concentration in the liquid phase significantly increases. This also shows that more CO_2 is dissolved in ethyl acetate at 7.39 MPa than at atmospheric pressure, which confirms that the solubility of CO_2 in ethyl acetate increases with increasing pressure.

Fig. 3a also shows that, when the pressure increases from atmospheric pressure to 7.39 MPa, the intensity of the $\nu_{C=O}$ absorption peak at 1745 cm^{-1} and the intensity of the –CH– absorption peak at 2985 cm^{-1} are significantly weakened. This occurs because, when the pressure rises, more CO_2 is dissolved in the ethyl acetate liquid, thus diluting the ethyl acetate liquid, causing the concentration of the ethyl acetate liquid to decrease and the intensity of the ethyl acetate absorption peak to decrease.

Fig. 3b shows the FTIR spectra of the $\nu_{C=O}$ absorption peak of ethyl acetate in the CO_2–ethyl acetate system from atmospheric pressure to 7.39 MPa at 308.15 K. When the liquid

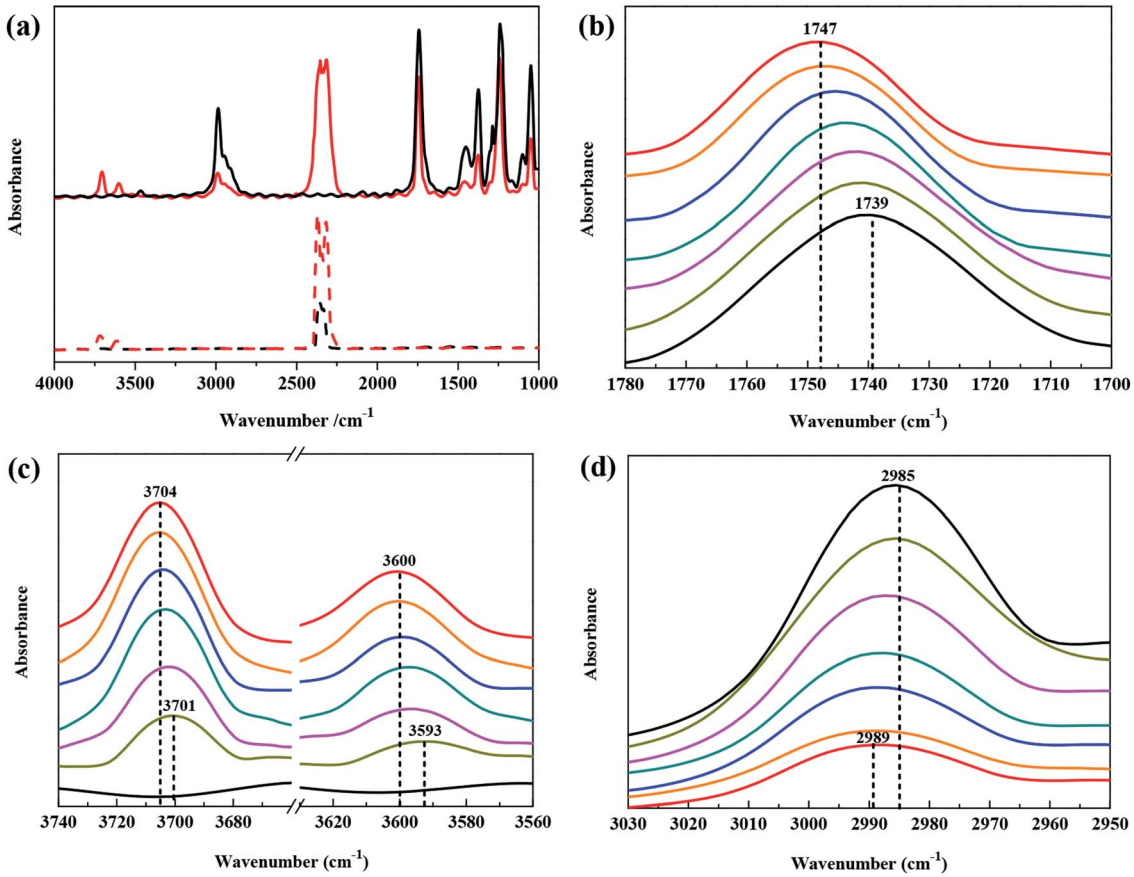

Fig. 3 FTIR spectra of CO_2–ethyl acetate system under different pressure conditions: (a) full spectrum; (b) the $\nu_{C=O}$ region of ethyl acetate; (c) the combination modes $2\nu_2 + \nu_3$ and $\nu_1 + \nu_3$ regions of CO_2 molecules; (d) the ν_{-CH_3} region of ethyl acetate. (—) ambient pressure, (—) 1.89 MPa, (—) 3.72 MPa, (—) 4.67 MPa, (—) 5.65 MPa, (—) 6.56 MPa, (—) 7.39 MPa, (- - -) raw CO_2 at ambient pressure, (- - -) raw CO_2 at 7.40 MPa.

system is under atmospheric pressure, the position of the carbonyl absorption peak is 1739 cm^{-1}; when the pressure rises to 7.39 MPa, the position of the carbonyl absorption peak gradually shifts to 1747 cm^{-1}. As the pressure is increased, the position of the carbonyl absorption peak shifts to a high wavenumber by 8 cm^{-1}. A decreased intermolecular force will cause an absorption peak to shift to a high wavenumber in the *in situ* FTIR spectrum.[44–46] Therefore, the abovementioned results indicate that, in the process of injecting CO_2 and as the pressure increases, more CO_2 molecules enter the ethyl acetate liquid, and the intermolecular force between the ethyl acetate molecules decreases, resulting in an increase in the force constant of the carbonyl bond. As a result, the position of the carbonyl absorption peak shifts toward a high wavenumber.

Fig. 3c shows the FTIR spectra (the combination modes $2\nu_2 + \nu_3$ and $\nu_1 + \nu_3$ stretching vibrations of the CO_2 molecule) of the CO_2–ethyl acetate system at 308.15 K when the pressure increased from atmospheric pressure to 7.39 MPa. Fig. 3c shows that, at 1.89 MPa, the positions of the $2\nu_2 + \nu_3$ and $\nu_1 + \nu_3$ CO_2 absorption peaks are 3701 cm^{-1} and 3593 cm^{-1}, respectively. When the pressure is increases to 7.39 MPa, the positions of these two absorption peaks shift to 3704 cm^{-1} and 3600 cm^{-1}. This result indicates that, when the pressure is increased from atmospheric pressure to 7.39 MPa, the absorption peaks of the CO_2–ethyl acetate system at 3700 cm^{-1} and 3600 cm^{-1} shift to higher wavenumbers by 3 cm^{-1} and 7 cm^{-1}, respectively. Due to an increase in the concentration, the FTIR absorption peak of pure CO_2 will increase with an increase in the pressure, but the position of the peak will not change.[47] When the pressure is 7.5 MPa, the absorption peak positions of pure CO_2 at these two locations are 3718 cm^{-1} and 3614 cm^{-1}.[30] Therefore, in the CO_2–ethyl acetate system, with an increase in the pressure, the interaction between the ethyl acetate molecules and CO_2 molecules leads to an increase in the force constant of CO_2, and the position of the FTIR CO_2 absorption peak shifts to a higher wavenumber.

Fig. 3d shows the absorption peaks (at approximately 2900 cm^{-1}) attributed to the $-CH_3$ groups in ethyl acetate in the CO_2–ethyl acetate system at 308.15 K when the pressure increases from atmospheric pressure to 7.39 MPa. These $-CH_3$ peaks are located at 2985 cm^{-1} and 2989 cm^{-1} at atmospheric pressure and at 7.39 MPa, respectively. As the pressure increases, the $-CH_3$ absorption peak shifts to a high wavenumber by 4 cm^{-1}. This result indicates that, with increasing pressure, more CO_2 enters the liquid molecules of ethyl acetate, which not only affects the interaction between the ethyl acetate molecules but also increases the force constant of the C–H bond

Table 1 The variation of the functional group high frequency offset of CO_2-different ester system with chain length under the same conditions

Ester type	CO_2 (3700 cm^{-1}) shift/cm^{-1}	CO_2 (3600 cm^{-1}) shift/cm^{-1}	$-CH_3$ (2900 cm^{-1}) shift/cm^{-1}	C=O (1700 cm^{-1}) shift/cm^{-1}
Ethyl acetate	3	7	4	8
Propyl propionate	3	5	2	5
Butyl butyrate	1	2	—	3

in the $-CH_3$ group. Therefore, the infrared absorption peak of $-CH_3$ shifts toward a high wavenumber.

Fig. S1 and S2† show the FTIR absorption spectra of the CO_2–propyl propionate system and CO_2–butyl butyrate system under different pressure conditions, respectively. The infrared spectra analysis of the three systems under the same conditions shows that, for the same pressure variation range, the length of the hydrocarbon chains has a significant impact on the shift of the absorption peaks of various functional groups of the system, as shown in Table 1. Table 1 shows that, under the same pressure variation condition, as the ester hydrocarbon chain length increases, the shift of the CO_2 absorption peak at 3600 cm^{-1} and the shift of the carbonyl absorption peak at 1700 cm^{-1} gradually decrease. The solubility and volume expansion analyses show that the ester chain length greatly affects the solubility of CO_2 in the ester and the volume expansion coefficient of the CO_2–ester system. The longer the chain length, the more difficult it is for CO_2 to dissolve and the smaller the volume expansion coefficient. The *in situ* infrared spectra show that the CO_2 absorption peak shift and carbonyl absorption peak shift are smaller in the esters with longer hydrocarbon chains, indicating that the longer the chain length, the more unfavorable it is for CO_2 to disperse in the ester liquid and the more difficult it is for CO_2 to enter the ester liquid to break the structure between the ester molecules. This also explains the lower solubility of CO_2 in long-chain esters under the same conditions and the smaller volume expansion of the CO_2-long-chain ester system.

3.3. Microscopic dispersion state of CO_2 in the ester liquids

The results of this study show that, as the pressure increases, the infrared absorption peak of CO_2 and the absorption peaks characteristic of the ester functional groups shift, which indicates that CO_2 is likely to interact with ester molecules. In addition, the interactions between CO_2 and ester molecules increase with the increasing of pressure. The CO_2 and ester molecules can have many different interaction modes.[48–50] The C atoms in the CO_2 molecule and the O atom in the carbonyl group of the ester molecule interact *via* Lewis acid–Lewis base (LA–LB) modes. A proton on the α-C on the alcohol side of the ester molecule and an O atom in CO_2 interact in the form of C–H···O. A proton on the α-C on the carbonyl side of the ester molecule and an O atom in CO_2 interact in the form of C–H···O. Taking ethyl acetate as an example, a specific interaction between the CO_2 and ethyl acetate molecules is shown in Fig. 4.

Based on the *in situ* infrared data analysis of CO_2 + ethyl acetate system under different pressures, the possible dispersion process of CO_2 in ethyl acetate can be inferred as follows (Fig. 5). In the ethyl acetate liquid, the ethyl acetate molecules form a network structure with three low-stability interactions (Fig. 5a). As the pressure increases, the solubility of CO_2 in the ethyl acetate liquid continuously increases, and the carbonyl absorption peak of the ethyl acetate molecules gradually shifts to a higher wavenumber, and the force constant of the carbonyl group gradually increases, indicating that the interactions between the ethyl acetate molecules gradually weaken. As increasing numbers of CO_2 molecules enter into the ethyl acetate liquid, the distance between the ethyl acetate molecules becomes larger. In the microscopic state, the original network structure of the ethyl acetate molecules is destroyed, and some of the ethyl acetate molecules are present as single molecules in

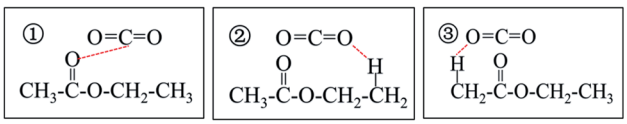

Fig. 4 Types of interaction between CO_2 and ethyl acetate molecules.

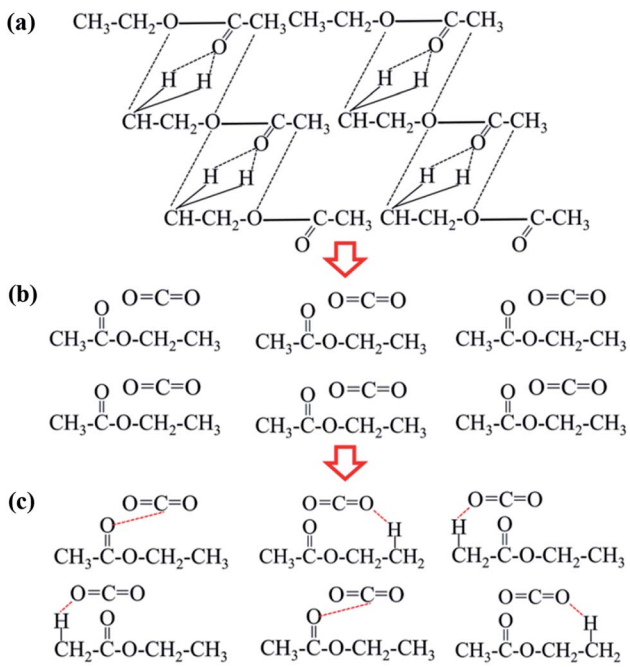

Fig. 5 Schematic of intermolecular interaction of CO_2 and ethyl acetate from ambient pressure to supercritical conditions: (a) ambient pressure; (b) 2.50 MPa; (c) the supercritical condition of CO_2.

the ethyl acetate system (Fig. 5b). CO_2 molecules form interactions with ethyl acetate through three non-covalent bonds, furthering disassembling the network structure of ethyl acetate. When supercritical conditions are reached, non-covalent bonds form between the CO_2 and ethyl acetate molecules, resulting in a completely dissociated ethyl acetate network structure (Fig. 5c).

4. Conclusions

In this work, the phase equilibrium data and FTIR spectra for the CO_2 and ester solvents mixtures under different pressures were obtained with a static analytical method using the PVT instrument and improved *in situ* infrared spectrometer under different pressure. At the same temperature, the CO_2 solubility and volume expansion coefficient of the CO_2–ester liquid system increase with increasing pressure. Longer hydrocarbon chains are associated with greater intermolecular forces, which can decrease the solubility of CO_2 in the ester liquid and decrease the volume expansion of the system. For the CO_2–ester liquid system, as the pressure increases, the infrared absorption peaks of CO_2 and the carbonyl group of the ester molecules gradually shift to higher wavenumbers, and the longer the hydrocarbon chain is, the smaller the shift. The microscopic dispersion state of CO_2 in ester solvents was further described based on the experimental results from the perspective of intermolecular interactions of the CO_2 molecules and ester molecules. Under supercritical CO_2 conditions, CO_2 molecules form interactions with ethyl acetate through three non-covalent bonds, resulting in the original network structure of the ethyl acetate molecules is destroyed. This study will enhance the understanding of the dispersion properties of CO_2 and ester solvents mixtures and facilitate their applications.

Conflicts of interest

There are no conflicts to declare.

Acknowledgements

This work was supported by the National Natural Science Foundation of China (51774302), National Key Technologies R&D Program of China (2017ZX05009-004) and National Natural Science Foundation of China (21503274).

References

1 H. Sovová, L. Opletal, M. Bártlová, M. Sajfrtová and M. Křenková, Supercritical fluid extraction of lignans and cinnamic acid from Schisandra chinensis, *J. Supercrit. Fluids*, 2007, **42**, 88–95.

2 S. Cavero, M. R. García-Risco, F. R. Marín, L. Jaime, S. Santoyo, F. J. Señoráns, G. Reglero and E. Ibañez, Supercritical fluid extraction of antioxidant compounds from oregano chemical and functional characterization via LC-MS and in vitro assays, *J. Supercrit. Fluids*, 2006, **38**, 62–69.

3 E. Reverchon and I. De Marco, Supercritical fluid extraction and fractionation of natural matter, *J. Supercrit. Fluids*, 2006, **38**, 146–166.

4 R. F. Rodrigues, A. K. Tashima, R. M. S. Pereira, R. S. Mohamed and F. A. Cabral, Coumarin solubility and extraction from emburana (Torresea cearensis) seeds with supercritical carbon dioxide, *J. Supercrit. Fluids*, 2008, **43**, 375–382.

5 G. L. Filho, V. V. De Rosso, M. A. A. Meireles, P. T. V. Rosa, A. L. Oliveira, A. Z. Mercadante and F. A. Cabral, Supercritical CO_2 extraction of carotenoids from pitanga fruits (Eugenia uniflora L.), *J. Supercrit. Fluids*, 2008, **46**, 33–39.

6 C. R. Piantino, F. W. B. Aquino, L. A. Follegatti-Romero and F. A. Cabral, Supercritical CO_2 extraction of phenolic compounds from Baccharis dracunculifolia, *J. Supercrit. Fluids*, 2008, **47**, 209–214.

7 D. Cossuta, B. Simándi, E. Vági, J. Hohmann, A. Prechl, É. Lemberkovics, Á. Kéry and T. Keve, Supercritical fluid extraction of Vitex agnus castus fruit, *J. Supercrit. Fluids*, 2008, **47**, 188–194.

8 P. M. Jarrell, C. E. Fox, M. H. Stein and S. L. Webb, *Practical aspects of CO_2 flooding, Monograph Series*, Society of Petroleum Engineers, 2002.

9 M. Cao and Y. Gu, Oil recovery mechanisms and asphaltene precipitation phenomenon in immiscible and miscible CO_2 flooding processes, *Fuel*, 2013, **109**, 157–166.

10 C. Or, K. Sasaki, Y. Sugai, M. Nakano and M. Imai, Swelling and viscosity reduction of heavy oil by CO_2-gas foaming in immiscible condition, *SPE Reservoir Eval. Eng.*, 2016, **19**, 294–304.

11 S. M. Seyyedsar and M. Sohrabi, Visualization observation of formation of a new oil phase during immiscible dense CO_2 injection in porous media, *J. Mol. Liq.*, 2017, **241**, 199–210.

12 M. Lashkarbolooki, M. Riazi and S. Ayatollahi, Experimental investigation of dynamic swelling and Bond number of crude oil during carbonated water flooding; effect of temperature and pressure, *Fuel*, 2018, **214**, 135–143.

13 S. Le Van and B. H. Chon, Effects of salinity and slug size in miscible CO_2 water-alternating-gas core flooding experiments, *J. Ind. Eng. Chem.*, 2017, **52**, 99–107.

14 T. Huang, X. Zhou, H. Yang, G. Liao and F. Zeng, CO_2 flooding strategy to enhance heavy oil recovery, *Petroleum*, 2017, **3**, 68–78.

15 Y. Yang, X. Li, P. Guo, Y. Zhuo and Y. Sha, Improving oil recovery in the CO_2 flooding process by utilizing nonpolar chemical modifiers, *Chin. J. Chem. Eng.*, 2016, **24**, 646–650.

16 A. Rostami, M. Arabloo, M. Lee and A. Bahadori, Applying SVM framework for modeling of CO_2 solubility in oil during CO_2 flooding, *Fuel*, 2018, **214**, 73–87.

17 Z. Yang, W. Wu, Z. Dong, M. Lin, S. Zhang and J. Zhang, Reducing the minimum miscibility pressure of CO_2 and crude oil using alcohols, *Colloids Surf., A*, 2019, **568**, 105–112.

18 Z. Yang, M. Li, B. Peng, M. Lin and Z. Dong, Dispersion property of CO_2 in oil. 2: volume expansion of CO_2 +

organic liquid at near-critical and supercritical conditions of CO_2, *J. Chem. Eng. Data*, 2012, **57**, 1305–1311.

19 S. N. Joung, C. W. Yoo, H. Y. Shin, S. Y. Kim, K. Yoo, C. S. Lee and W. S. Huh, Measurements and correlation of high-pressure VLE of binary CO_2-alcohol systems (methanol, ethanol, 2-methoxyethanol and 2-ethoxyethanol), *Fluid Phase Equilib.*, 2001, **185**, 219–230.

20 C. J. Chang, K. Chiu and C. Day, A new apparatus for the determination of P-x-y diagrams and Henry's constants in high pressure alcohols with critical carbon dioxide, *J. Supercrit. Fluids*, 1998, **12**, 223–237.

21 H. Lee, S. Yong Mun and H. Lee, High-pressure phase equilibria for the carbon dioxide-2-methyl-1-butanol, carbon dioxide–2-methyl-2-butanol, carbon dioxide–2-methyl-1-butanol–water, and carbon dioxide–2-methyl-2-butanol–water systems, *Fluid Phase Equilib.*, 1999, **157**, 81–91.

22 K. Gauter, R. A. Heidemann and C. J. Peters, Modeling of fluid multiphase equilibria in ternary systems of carbon dioxide as the near-critical solvent and two low-volatile solutes, *Fluid Phase Equilib.*, 1999, **158–160**, 133–141.

23 J. Yu, S. Wang and Y. Tian, Experimental determination and calculation of thermodynamic properties of CO_2 + octane to high temperatures and high pressures, *Fluid Phase Equilib.*, 2006, **246**, 6–14.

24 E. N. Lay, V. Taghikhani and C. Ghotbi, Measurement and correlation of CO_2 solubility in the systems of CO_2 + toluene, CO_2 + benzene, and CO_2 + n-hexane at near-critical and supercritical conditions, *J. Chem. Eng. Data*, 2006, **51**, 2197–2200.

25 Z. Yang, M. Li, B. Peng, M. Lin and Z. Dong, Aggregation of CO_2 and organic liquid molecules at near critical and supercritical condition of CO_2, *J. Dispersion Sci. Technol.*, 2014, **35**, 168–174.

26 Z. Yang, M. Li, B. Peng, M. Lin and Z. Dong, Dispersion property of CO_2 in oil. Part 3: aggregation of CO_2 molecule in organic liquid at near critical and supercritical condition of CO_2, *J. Dispersion Sci. Technol.*, 2014, **35**, 143–149.

27 A. V. Ewing, A. A. Gabrienko, S. V. Semikolenov, K. A. Dubkov and S. G. Kazarian, How do intermolecular interactions affect swelling of polyketones with a differing number of carbonyl groups? An in situ ATR-FTIR spectroscopic study of CO_2 sorption in polymers, *J. Phys. Chem. C*, 2015, **119**, 431–440.

28 S. P. Nalawade, F. Picchioni, J. H. Marsman and L. P. B. M. Janssen, The FT-IR studies of the interactions of CO_2 and polymers having different chain groups, *J. Supercrit. Fluids*, 2006, **36**, 236–244.

29 A. Rajendran, B. Bonavoglia, N. Forrer, G. Storti, M. Mazzotti and M. Morbidelli, Simultaneous measurement of swelling and sorption in a supercritical CO_2–poly(methyl methacrylate) system, *Ind. Eng. Chem. Res.*, 2005, **44**, 2549–2560.

30 L. Peng, Z. Yang, M. Li, M. Lin and Z. Dong, Dispersion properties of CO_2 and polar organic solvents with the same alkyl chain length mixtures using in situ FTIR spectroscopy, *J. Supercrit. Fluids*, 2018, **135**, 234–244.

31 H. S. Byun, M. Y. Choi and J. S. Lim, High-pressure phase behavior and modeling of binary mixtures for alkyl acetate in supercritical carbon dioxide, *J. Supercrit. Fluids*, 2006, **37**, 323–332.

32 S. Sima, V. Feroiu and D. Geană, New high pressure vapor-liquid equilibrium data and density predictions for carbon dioxide + ethyl acetate system, *Fluid Phase Equilib.*, 2012, **325**, 45–52.

33 A. Chrisochoou, K. Schaber and U. Bolz, Phase equilibria for enzyme-catalyzed reactions in supercritical carbon dioxide, *Fluid Phase Equilib.*, 1995, **108**, 1–14.

34 Y. L. Tian, H. G. Zhu, Y. Xue, Z. H. Liu and L. Yin, Vapor-liquid equilibria of the carbon dioxide + ethyl propanoate and carbon dioxide + ethyl acetate systems at pressure from 2.96 MPa to 11.79 MPa and temperature from 313 K to 393 K, *J. Chem. Eng. Data*, 2004, **49**, 1554–1559.

35 A. Kordikowski, A. P. Schenk, R. M. Van Nielen and C. J. Peters, Volume expansions and vapor-liquid equilibria of binary mixtures of a variety of polar solvents and certain near-critical solvents, *J. Supercrit. Fluids*, 1995, **8**, 205–216.

36 H. Li, R. Zhu, W. Xu, H. Xu, Z. Dong and Y. Tian, Vapor-liquid equilibrium data of (carbon dioxide + methyl propionate) and (carbon dioxide + propyl propionate) at pressures from (1.00 to 12.00) MPa and temperatures from (313.0 to 373.0) K, *J. Chem. Eng. Data*, 2009, **54**, 1510–1517.

37 M. Kato, D. Kodama, M. Sato and K. Sugiyama, Volumetric behavior and saturated pressure for carbon dioxide + ethyl acetate at a temperature of 313.15 K, *J. Chem. Eng. Data*, 2006, **51**, 1031–1034.

38 Y. C. Tien, C. S. Su, L. H. Lien and Y. P. Chen, Recrystallization of erlotinib hydrochloride and fulvestrant using supercritical antisolvent process, *J. Supercrit. Fluids*, 2010, **55**, 292–299.

39 A. K. Baev, *Specific intermolecular interactions of organic compounds*, Springer Science & Business Media, 2012.

40 I. A. Vasil'ev and V. M. Petrov, *Thermodynamic properties of oxygen-containing organic compounds*, Khimiya, Leningrad, 1984.

41 E. Mosconi, C. Quarti, T. Ivanovska, G. Ruani and F. De Angelis, Structural and electronic properties of organo-halide lead perovskites: a combined IR-spectroscopy and ab initio molecular dynamics investigation, *Phys. Chem. Chem. Phys.*, 2014, **16**, 16137–16144.

42 B. E. Poling, J. M. Prausnitz and J. P. O'connell, *The properties of gases and liquids*, Mcgraw-hill, New York, 2001.

43 Y. Lebedev and E. A. Miroschnichenko, *Thermochemistry of the vaporization of organic compounds. The vaporization and sublimation enthalpy and saturated pressure*, Nauka, Moscow, 1981.

44 P. S. Makashir and E. M. Kurian, Spectroscopic and thermal studies on the decomposition of l,3,5-triamino-2,4,6-trinitrobenzene (TATB), *J. Therm. Anal.*, 1996, **46**, 225–236.

45 M. Pravica, B. Yulga, S. Tkachev and Z. Liu, High-pressure far- and mid-infrared study of 1,3,5-triamino-2,4,6-trinitrobenzene, *J. Phys. Chem. A*, 2009, **113**, 9133–9137.

46 G. Herzberg, *Molecular spectra and molecular structure II. Infrared and Raman spectra of polyatomic molecules*, Van Nostrand, New York, 1945.
47 L. Peng, Dispersion property of CO_2 in heavy crude oil and polar organic liquids, Doctoral thesis, China University of Petroleum (Beijing), China, 2017.
48 Y. Yuan and A. S. Teja, Quantification of specific interactions between CO_2 and the carbonyl group in polymers via ATR-FTIR measurements, *J. Supercrit. Fluids*, 2011, **56**, 208–212.
49 Y. Akiyama, S. Fujita, H. Senboku, C. M. Rayner, S. A. Brough and M. Araia, An in situ high pressure FTIR study on molecular interactions of ketones, esters, and amides with dense phase carbon dioxide, *J. Supercrit. Fluids*, 2008, **46**, 197–205.
50 C. Drohmann and E. J. Beckman, Phase behavior of polymers containing ether groups in carbon dioxide, *J. Supercrit. Fluids*, 2002, **22**, 103–110.